Sustainable Food Technology

ROYAL SOCIETY OF CHEMISTRY

PAPER

View Article Online
View Journal | View Issue

Cite this: *Sustainable Food Technol.*, 2025, **3**, 1901

Sustainable antimicrobial packaging films: effectiveness of epsilon-poly-L-lysine in PLA/PBAT blend films

Pullarkad Bharathan Smrithy,[a] Johnsy George, *[a] Aksalamol Pallivathukkal Raju,[a] Muhammed Riyaz Guthige,[a] Gowdahalli Mantelingachar Chandrika,[a] Venugopal Vasudevan,[a] Radhika Madan Urs[b] and Ranganathan Kumar[a]

With the rising demand for environmentally friendly and sustainable food packaging solutions, there is growing interest in developing advanced compostable polymers with improved functional attributes. However, compostable polymers such as polylactic acid (PLA) exhibit certain drawbacks such as brittleness, which limit their application in flexible packaging. A promising strategy to address these limitations is blending PLA with polybutylene adipate terephthalate (PBAT), resulting in a compostable blend with well-balanced properties. The present work aims to develop active packaging films using PLA/PBAT blends, with the inclusion of different amounts (1–5 wt%) of the natural antimicrobial compound ε-poly-L-lysine (ε-PL). The films were produced using twin-screw blown film extrusion and evaluated for their mechanical, morphological, barrier and antimicrobial properties. The presence of ε-PL within the PLA/PBAT matrix was verified by Fourier-transform infrared spectroscopy (FTIR) analysis, which revealed characteristic absorption peaks in the 1500–1600 cm^{-1} range. Surface morphology represents heterogeneous dispersion of ε-PL in the PLA/PBAT matrix. Contact angle analysis revealed a progressive increase in surface hydrophilicity with higher ε-PL content, decreasing from 61.72° to 47.73°. X-ray diffraction (XRD) showed a reduction in crystallinity as the ε-PL concentration increased, while differential scanning calorimetry (DSC) provided insights into thermal transitions. Incorporation of ε-PL in the polymer blend led to a reduction in both oxygen and water vapor barrier properties. The antimicrobial effectiveness of the films was assessed against *Staphylococcus aureus*, with the 5 wt% ε-PL film exhibiting antibacterial activity (30.6 mm zone of inhibition). Release kinetics analysis indicated that ε-PL release followed Fickian diffusion, with the Higuchi model offering the best fit for the data (R^2 = 0.98). When bananas were stored in PLA/PBAT blend films containing ε-PL, their quality was better maintained compared to both unpackaged bananas and those packed in control films. These findings suggest that PLA/PBAT films incorporated with ε-PL hold strong potential as more sustainable active packaging materials offering enhanced food safety and extended shelf life.

Received 20th June 2025
Accepted 14th August 2025

DOI: 10.1039/d5fb00286a

rsc.li/susfoodtech

Sustainability spotlight

This study addresses some of the challenges in replacing non-degradable conventional plastic based food packaging materials with more sustainable PLA based materials. This approach fosters a circular materials economy and directly supports the UN Sustainable Development Goals on Responsible Consumption and Production. This is achieved by advancing resource efficiency and driving the use of more sustainable materials for packaging and related applications.

1 Introduction

Packaging is essential in the food industry as it safeguards food safety, extends shelf life and enhances consumer satisfaction. It helps maintain the nutritional value and safety of food items by acting as a barrier against light, air, moisture, and contaminants. Effective packaging reduces food waste, prevents spoilage, and supports compliance with food safety regulations by inhibiting microbiological growth and chemical migration. Sustainable packaging options, such as biopolymers, are gaining increasing popularity due to growing environmental concerns. These materials play a vital role in reducing plastic waste and promoting a circular economy.[1] Several biopolymers, including PLA, polyhydroxyalkanoates (PHAs), cellulose, starch, other water soluble polymers, *etc.*, can be used for food

[a]*Food Engineering and Packaging Technology Division, Defence Institute of Bio-Defence Technology, Mysore, 570011, Karnataka, India. E-mail: g.johnsy@gmail.com*
[b]*Food Microbiology Division, Defence Institute of Bio-Defence Technology, Mysore, 570011, Karnataka, India*

packaging.[2–4] Of these, PLA is especially notable because it is easy to process using standard plastic manufacturing techniques and is compostable, making it a leading candidate for sustainable food packaging materials. PLA is a thermoplastic polyester produced by fermenting natural starches such as cassava, sugarcane and corn. Although PLA exhibits good tensile strength and transparency, its use in food packaging is restricted due to its inherent brittleness and limited flexibility.[5] Recent advances have shown that blending PLA with flexible, compostable polymers such as PBAT and incorporating additives like chain extenders or plasticizers enhances both processability and end-use performance, broadening its applicability in sustainable food packaging.[6]

The development of PLA-based compostable antimicrobial packaging is a trending topic in the food packaging sector, as it promotes environmental sustainability and enhances food safety.[7] Antimicrobial packaging, a form of active packaging technology, extends food shelf life by inhibiting bacterial growth on the food surface through controlled release mechanisms. Recent developments in antimicrobial active packaging films focus on integrating natural and synthetic antimicrobial agents into biopolymer matrices to enhance food safety and extend shelf life. While synthetic antimicrobial agents such as silver nanoparticles, quinolones, and sulfonamides have been widely used, concerns over their toxicity and regulatory restrictions have shifted attention toward natural alternatives. On the other hand, some of the natural antimicrobial substances such as plant extracts and essential oils (including clove, cinnamon, peppermint, thymol, *etc.*) present challenges such as low thermal stability, volatility, and sensory issues.[8,9] In this context, ε-PL, a naturally occurring antibacterial polypeptide made by microbial fermentation, stands out as a suitable antimicrobial agent. It is widely used in food preservation, biomedical and pharmaceutical applications.[10,11] ε-PL efficiently inhibits the growth of molds, Gram-positive and Gram-negative bacteria, yeast, and other microorganisms by disrupting cell walls and inhibiting enzymatic activity.[12] The Food and Drug Administration (FDA) and European Food Safety Authority (EFSA) have recognized ε-PL as a safe food preservative that decomposes naturally, making it an appropriate antibacterial agent for active and sustainable packaging.[13] Several studies have explored the release kinetics of ε-PL from biodegradable polymeric film matrices such as alginate, chitosan, polyvinyl alcohol and starch aiming to optimize its antimicrobial performance for various applications.[14] For example, incorporating ε-PL into fish gelatin–chitosan matrices with cinnamaldehyde as a cross-linker resulted in food packaging films with antimicrobial activity.[15] Antimicrobial ε-PL incorporating sodium alginate microspheres were reportedly used to prolong the shelf life of fruit.[16] Tea polyphenols with ε-PL core–shell microcapsules were also developed for their application in the preservation of food.[17]

In this study, we first optimized the concentration of PBAT required to blend with PLA to achieve reasonable elongation properties in the resulting films. The optimum concentration of ε-PL necessary to impart effective antimicrobial properties to PLA/PBAT blend films was determined. Additionally, the study systematically investigated the influence of ε-PL on the physicochemical, thermal and antimicrobial properties of the blend films, with a particular focus on their potential applications in food packaging. To evaluate the efficacy of these antimicrobial films, bananas were packaged using the developed films and their quality deterioration during ripening at room temperature storage was monitored. This approach provides practical insights into the performance of PLA/PBAT-based antimicrobial packaging for extending the shelf life of fresh produce.

2 Materials and methods

2.1. Materials

PLA biopolymer, Ingeo® 2003D, characterized by a D-isomer content of 4%, specific gravity 1.24, Mn of 114 300 g mol^{-1}, M_w of 181 700 g mol^{-1} and melt flow rate (MFR) of 6 g/10 min was obtained from NatureWorks LLC (Minneapolis, MN, USA). PBAT grade Ecoflex®, a compostable polyester, with specific gravity 1.26 and MFR 3–5 g/10 min at 190 °C was purchased from BASF (Ludwigshafen, Germany). 100% A-grade ε-PL was obtained from Bimal Pharma Pvt. Ltd., Mumbai.

2.2. Masterbatch development

A PLA/PBAT (70/30) blend masterbatch was prepared to achieve complete mixing and uniform dispersion of additives within the blend. Prior to compounding, PLA/PBAT (70/30) pellets were dried in a hot air oven for 4 h at 75 °C (Memmert UFE-500, Germany). Different concentrations of ε-PL (1, 2, 3, 4 and 5 wt%) were physically mixed with the PLA/PBAT blend for 15 min using a ribbon blender. The resulting blend was then extruded in a twin screw polymer extruder (Dr Collin ZK 25T, Teach Line, Germany). The temperature profile for the four sections of the barrel was set to 155 °C/160 °C/165 °C/170 °C, which is required to adequately melt and process PLA and PBAT. Since ε-PL is thermally stable up to 300 °C with no significant loss of its antimicrobial properties or material integrity, it was directly added to the masterbatch during extrusion. The extrudate was subsequently pelletized to produce masterbatch granules, which were sealed and stored at room temperature until further processing by blown film extrusion.

2.3. Fabrication of PLA/PBAT blend films

The blown film extrusion process was utilised to fabricate PLA/PBAT blend films, employing a twin screw extruder connected to a blown film unit (BL 400 E). Before extrusion, the prepared master batches were pre-dried at 75 °C in a hot air oven for 4 h to remove residual moisture. The screw speed was maintained between 30 and 35 rpm, and the take up ratio was 2. The temperature profile for the screw zone was set at 160 °C/165 °C/170 °C/175 °C and for the die zone was set at 170 °C/170 °C/170 °C/170 °C/170 °C respectively. The resulting blown films had an average thickness of 65 ± 5 μm for each film sample.

2.4. Characterization

2.4.1. FTIR spectroscopy. FTIR spectra were measured using an FTIR spectrophotometer (Thermo Scientific, Nicolet

Summit X, UK) fitted with an attenuated total reflectance (ATR) accessory. The analysis was conducted in ATR mode, utilizing a diamond crystal for the study. The film sample was kept in close contact with the crystal and scanning was performed across the 4000–400 cm^{-1} range by maintaining a resolution of 4 cm^{-1}. OMNIC Paradigm software was used to interpret the spectra.

2.4.2. Scanning electron microscopy (SEM). The surface morphology of the developed films was evaluated using a scanning electron microscope (Zeiss, EVO-LS 10, Germany). Surface and cross-sectional images were captured at a magnification of 500× and 1000× at an accelerated voltage of 20 kV. All samples were sputter coated (Emitech SC7620) by a thin layer of gold prior to imaging.

2.4.3. Contact angle measurement. The static contact angle of water in air was measured using the sessile drop technique with a contact angle meter (model: DMe-211 Plus, Kyowa Contact Angle Meters, Japan).[18] The film samples were trimmed into 10 cm × 10 cm squares and firmly positioned on the sampling stage. The sample stage was raised to delicately deposit a droplet of distilled water (2 ± 0.1 μL) onto each film substrate. The static contact angle for all samples was measured immediately after droplet deposition. Each measurement was preceded by a 2000 ms waiting period to allow droplet deposition. The image was obtained using a CMOS sensor camera having high-resolution with a built-in LED light source. Data analysis and contact angle determination were performed using FAMAS software. All measurements were carried out under controlled conditions of 50 ± 2% relative humidity (RH) and 23 ± 2 °C temperature. For every sample, at least 10 values were taken from various spots and their mean value was recorded.

2.4.4. DSC analysis. A differential scanning calorimeter (model: Discovery DSC 25, TA Instruments, USA) was used to assess the samples' thermal characteristics, such as their melting point (T_m), cold crystallization temperature (T_c), and glass transition temperature (T_g), using the heat–cool–heat procedure. The device was calibrated for heat flow and temperature by following a procedure which was previously reported.[19] Samples weighing between 5 and 10 mg were carefully placed in a Tzero aluminum pan, properly closed with a Tzero lid, and analyzed. The films were first heated to 200 °C from room temperature at 10 °C min^{-1}, cooled to −50 °C at the same rate to arrest polymer molecular activity, and then reheated to 200 °C at 10 °C min^{-1}. The resulting thermogram, plotting heat flow *versus* temperature, was analyzed to identify first- and second-order phase transitions like T_m, T_g, and T_c.

2.4.5. XRD analysis. An X-ray diffractometer (model: D2 Phaser, Bruker AXS, Germany) was used to evaluate the percentage crystallinity of the samples by analyzing their XRD spectra.[20] The measurements were carried out by scanning the samples over a diffraction angle (2θ) range of 6° to 70° using Cu Kα ($\lambda = 1.5406$ Å) radiation. The instrument was operated at 10 mA and 30 kV.

2.4.6. Oxygen transmission rate (OTR). OTR analysis was performed on the film samples using an oxygen transmission rate analyzer (Mocon Ox-Tran 2/22L, US) in compliance with ASTM D3985. Before testing, samples were conditioned in a desiccator at 0% RH for 48 h. Using a template, each sample was cut into an octagonal shape, and the test area was reduced to 5 cm^2 by masking with foil. The purging gas was a nitrogen-hydrogen combination (mixture of 98% N_2 and 2% H_2), and the carrier gas was 99.9% pure oxygen. The analysis was performed at 23 ± 2 °C and 0% RH.

2.4.7. Water vapor transmission rate (WVTR). Film samples underwent WVTR testing with a WVTR analyzer in accordance with ASTM F1249 (model: Permatran-W 3/33, Mocon, US). A template was used to cut each sample into a hexagon, and the test area was reduced to 5 cm^2 by masking with foil. The analysis was performed with 99.9% pure nitrogen gas as the purging gas. Testing was conducted at 37.8 ± 1 °C and 100% RH, ensuring accurate assessment of the films' barrier properties.

2.4.8. Mechanical properties. Using a universal testing machine (UTM) fitted with a 1 kN load cell, key mechanical parameters such as Young's modulus, tensile strength and percentage elongation were evaluated (model: LRX Plus, Lloyd Instruments, UK). Testing of all samples was performed in accordance with ASTM D882. In every test, the gauge length and cross-head speed were maintained at 100 mm and 50 mm min^{-1} respectively. Each sample was cut along the machine direction. The results represent the average values obtained from testing at least five samples for each condition.

2.4.9. Antimicrobial analysis. The film samples were evaluated for antibacterial activity against Gram-negative *Escherichia coli* (ATCC 10536) and Gram-positive *Staphylococcus aureus* (ATCC 700699) strains using the well diffusion method on Mueller–Hinton agar (MHA) medium. Film extracts were prepared by immersing film samples (1 cm × 1 cm) of equal weight in 5 mL of sterile distilled water and incubating at 37 °C for 24 h. The strains of bacteria were cultivated in nutrient medium at 37 °C for 24 h prior to testing. For inoculation, a sterilized cotton swab was immersed into the microbial culture and spread across the agar plates in four directions, rotating the plate 45° every time to ensure uniform coverage. A 12 mm diameter well was created in the agar, and 200 μL of the film extract was carefully added to the well using a micropipette (Nichipet EX II, Japan). The plates were then incubated at 37 °C for 24 h. Antibacterial activity was assessed by evaluating the zone of inhibition diameter around the sample well, and the results were reported as the growth inhibition diameter in millimeters.[21]

2.4.10. Release kinetics of ε-PL. The ε-PL release studies were carried out with a UV-visible spectrophotometer (model: Lambda 365, PerkinElmer, US) at a characteristic wavelength of 203 nm.[22] A calibration curve was constructed using standard ε-PL solutions. Film samples (5 × 5 cm^2) were immersed in 50 mL of distilled water. Samples (2 mL) were collected from the release medium at predetermined intervals of 0, 5, 10, 15, 30, 45, 60, 120, 180, and 240 min and each sample was replaced with 2 mL of fresh distilled water to preserve the total volume and concentration. The collected samples were analyzed using spectrophotometric methods. The data obtained were fitted to various models of release kinetics, including first-order

kinetics, the Higuchi model, zero-order kinetics, and the Korsmeyer–Peppas model, to study the release behavior of ε-PL.

2.4.11. Shelf life studies using packaged bananas. Fresh, uniformly ripe bananas were procured locally in Mysore, India, then cleaned and dried prior to packaging. The bananas were divided into three groups: the first group served as a control and remained unpackaged; the second group was packaged with PLA/PBAT blend films; and the third group was packaged with PLA/PBAT blend films containing ε-PL. All samples were stored at room temperature. The bananas were then evaluated for weight loss percentage, pH, texture profile analysis (TPA), color analysis, titratable acidity (TA) and total soluble solids (TSS).

2.4.12. TPA. A UTM equipped with a 20 N load cell was employed to measure the hardness of banana samples (model: LRX Plus Lloyd Instruments, UK). Sample penetration was performed using a 3 mm diameter cylindrical stainless steel probe. The test was conducted at a speed of 1 mm s^{-1}, with a penetration depth of 10 mm. The results were calculated from the average value obtained by testing at least three replicates for each sample.

2.4.13. Colour measurement. The color of the banana pulp was evaluated using a HunterLab colorimeter (ColorFlex EZ, USA). The color space coordinates for L^* (lightness), b^* (yellowness/blueness) and a^* (redness/greenness) were determined. Prior to analysis, standard black and white plates were used to calibrate the colorimeter.

2.4.14. Weight loss. A digital balance was used to record the daily weight of the packed banana and weight loss percentage was subsequently calculated.

2.4.15. TSS. A handheld refractometer was used to determine the TSS (Atago India Instruments Pvt. Ltd., Mumbai) by placing mashed banana pulp on the sample plate and the readings were expressed in °brix.

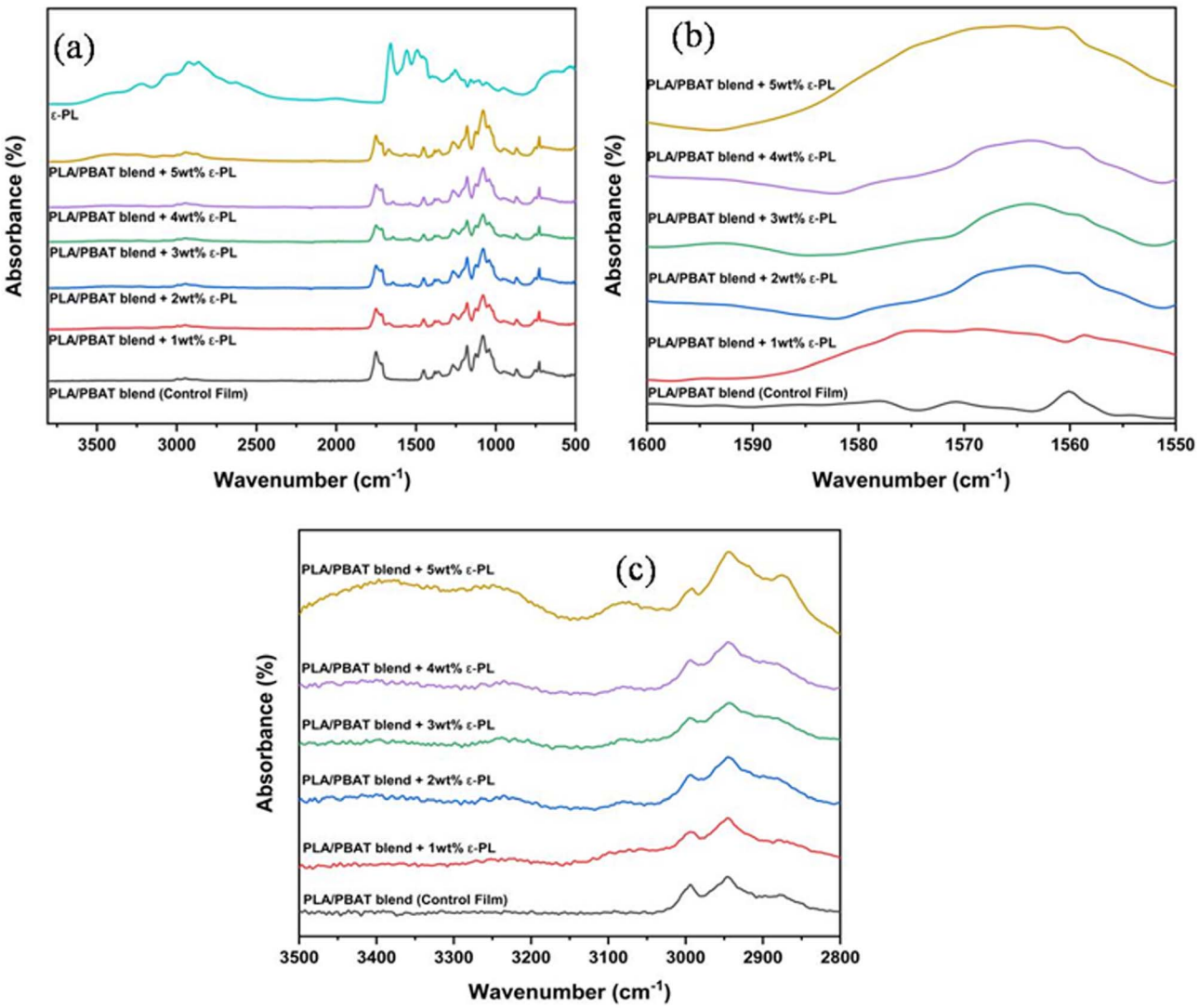

Fig. 1 (a) FTIR spectra of ε-PL, PLA/PBAT blend control film and PLA/PBAT blend films loaded with different weight percentages of ε-PL (1–5 wt%). (b) Enlarged view of the FTIR spectra in the 1550–1600 cm^{-1} regions. (c) Enlarged view of the FTIR spectra in the 2800–3500 cm^{-1} regions.

2.4.16. pH. An electronic pH meter (Horiba Scientific F-74G) was used to determine the sample's pH. Buffer was used to calibrate the pH meter at pH 4, 7, and 9. For pH measurements, banana samples (10 g) were homogenized in distilled water (50 mL).

2.4.17. TA. The TA was measured using acid–base titration. 10 g of blended banana pulp was combined with 50 mL of distilled water and filtered, and then 10 mL of the clear liquid was titrated with 0.1 N NaOH using an indicator (phenolphthalein). The endpoint was identified as a consistent pale pink color.[23] Titratable acidity was calculated and expressed as the percentage of malic acid, the major organic acid in banana.

2.4.18. Statistical analysis. Statistical analysis was carried out using IBM SPSS version 20.0 (SPSS Inc., Chicago, IL). One-way ANOVA was employed to evaluate differences among groups, and Tukey's *post hoc* test was used to identify significant pairwise comparisons at $p \leq 0.05$. The mean ± standard deviation (SD) represents the experimental outcomes.

3 Results and discussion

3.1. FTIR spectroscopy

The FTIR spectra presented in Fig. 1(a) clearly demonstrate the chemical structure of PLA/PBAT blend films containing 1–5 wt% of ε-PL. All films exhibited characteristic peaks corresponding to both PLA and PBAT. A strong absorption peak observed between 1752 and 1711 cm^{-1} corresponds to the stretching vibration characteristic of ester groups (C═O stretching) in both polymers.[24] The peak at around 1450 cm^{-1} corresponds to the C–H bending vibration of the methyl group in PLA, and this peak is a specific marker for PLA within the blend.[25] The 1270 cm^{-1} peak is related to the aromatic ester (C–O stretching) of PBAT.[26] Additionally, the doublet peak observed between 1380 and 1360 cm^{-1} is characteristic of the symmetric and asymmetric bending modes of the methyl group, commonly found in aliphatic polyesters such as PLA and PBAT.[26] The triplet peaks at 1120, 1081, and 1043 cm^{-1} are

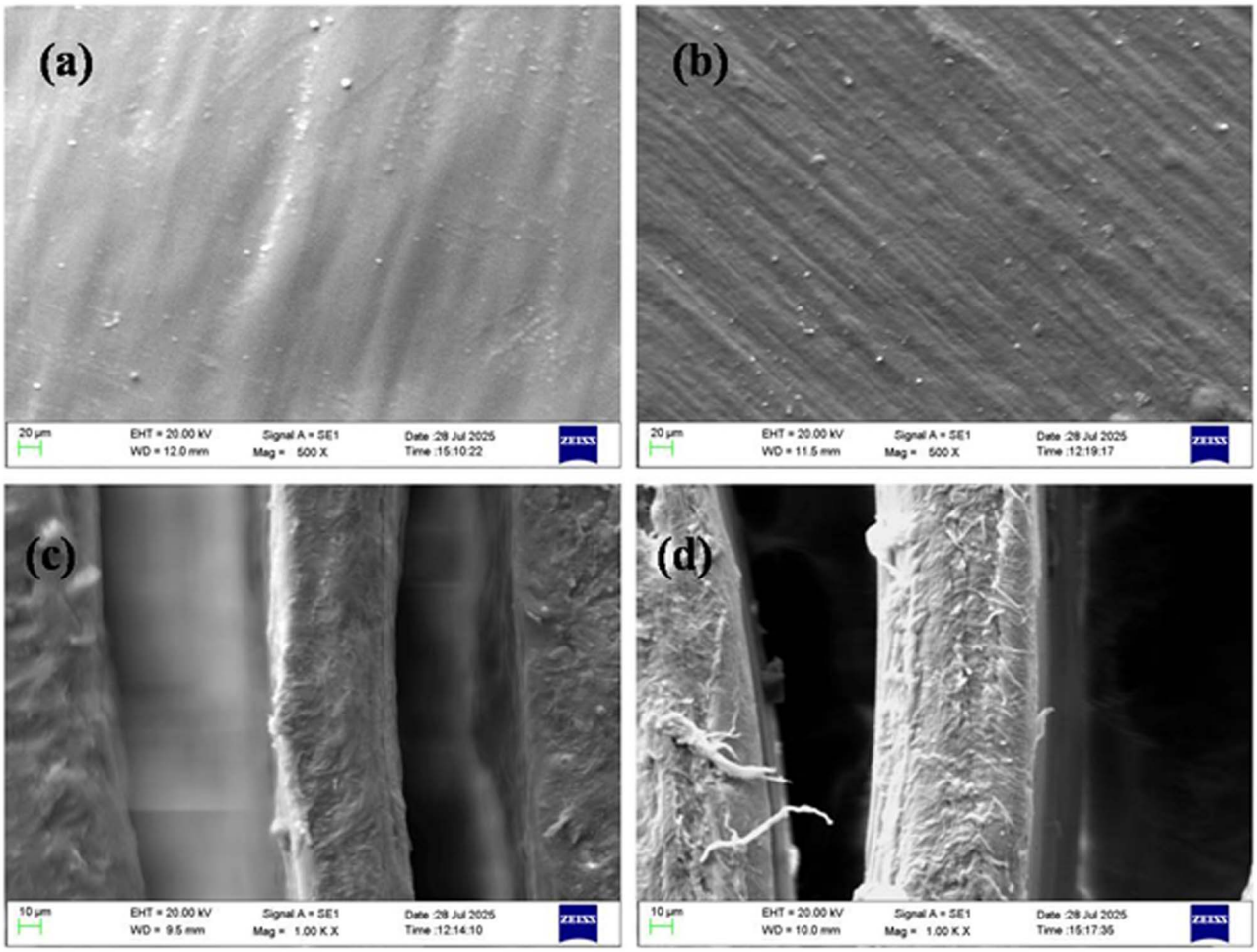

Fig. 2 SEM images of (a) PLA/PBAT blend control film and (b) PLA/PBAT blend + 4 wt% ε-PL film. (c) Cross-sectional image of the PLA/PBAT blend control film. (d) Cross-sectional image of the PLA/PBAT blend + 4 wt% ε-PL film.

attributable to the C–O and C–O–C stretching vibrations present in both PLA and PBAT.[27,28]

Notably, as the ε-PL content increases from 1 wt% to 5 wt%, a progressive increase in the intensity of the broad absorption band is visible in the 3200–3500 cm^{-1} regions, which is attributed to the O–H and N–H stretching vibrations.[29] This confirms the successful incorporation of ε-PL into the PLA/PBAT blend films, as these functional groups are characteristics of ε-PL. The presence of ε-PL is further supported by a slight increase in peak intensity in the 1500–1600 cm^{-1} area, associated with N–H bending vibrations of the amide groups.[30] Additionally no peak shifts were observed in the spectra, confirming that ε-PL was physically incorporated within the blend without forming any new covalent bonds. Overall, FTIR analysis suggests the presence of ε-PL in the blend films through physical interactions while maintaining the structural integrity of the PLA/PBAT blend. When hydrophilic antimicrobial agents such as ε-PL are physically incorporated into polymer films like PLA/PBAT, their migration to the film surface is significantly influenced by moisture. Upon exposure to moisture or high humidity, diffusion of the antimicrobial agent is facilitated, and it tends to migrate toward the surface, where it can directly interact with food–contact interfaces. This moisture-triggered migration enhances the effectiveness of hydrophilic antimicrobial agents because their activity depends on surface availability. Moisture from the environment or food products stimulates the agent's release, ensuring sustained antimicrobial activity precisely when and where it is most needed.

Table 1 Contact angle of PLA/PBAT blend control films and PLA/PBAT blend loaded films with different weight percentages of ε-PL (1–5 wt%)[a]

Sample name	Contact angle (°)
PLA/PBAT blend control film	72.23 ± 1.33^{d}
PLA/PBAT blend + 1 wt% ε-PL	61.72 ± 2.25^{c}
PLA/PBAT blend + 2 wt% ε-PL	55.06 ± 1.85^{b}
PLA/PBAT blend + 3 wt% ε-PL	53.09 ± 3.99^{b}
PLA/PBAT blend + 4 wt% ε-PL	50.35 ± 3.54^{ab}
PLA/PBAT blend + 5 wt% ε-PL	47.43 ± 0.28^{a}

[a] Values in the same column with different lowercase letters (a–d) are significantly different at $p \leq 0.05$. All values are expressed as the mean ± SD ($n = 10$).

3.2. Surface morphology

The surface morphology of PLA/PBAT blend films, both with and without ε-PL incorporation, was evaluated using SEM. Fig. 2 shows surface and cross-sectional SEM images of the control PLA/PBAT blend and the film containing 4 wt% ε-PL at 500× and 1000× magnification. The control PLA/PBAT blend film exhibits a relatively smooth surface with limited phase separation and no visible pores or cracks, indicating good film integrity. The cross-sectional image (Fig. 2(c)) of the control film reveals a compact and less heterogeneous internal structure, with no noticeable voids or phase boundaries, suggesting good dispersion of PBAT within the PLA matrix despite their inherent incompatibility.[31]

The film containing 4 wt% ε-PL shows a rougher surface morphology with small aggregated domains, indicating heterogeneous dispersion of ε-PL in the PLA/PBAT matrix. The increased surface roughness is consistent with the observed decrease in the water contact angle described in Section 3.3, reflecting enhanced film hydrophilicity. The cross-sectional morphology of the ε-PL loaded film is also rougher and more heterogeneous, with dispersed microdomains that may signify localized phase separation or ε-PL agglomerates. This suggests that ε-PL preferentially localizes at the PLA/PBAT interface or forms distinct inclusions within the matrix. Such structural changes could affect the film's mechanical and barrier properties. Overall, SEM analysis confirms that incorporation of ε-PL alters the surface and internal morphology of PLA/PBAT blend films. While ε-PL improves functionalities such as wettability and potentially enhances antibacterial activity by increasing surface availability, it also introduces minor morphological

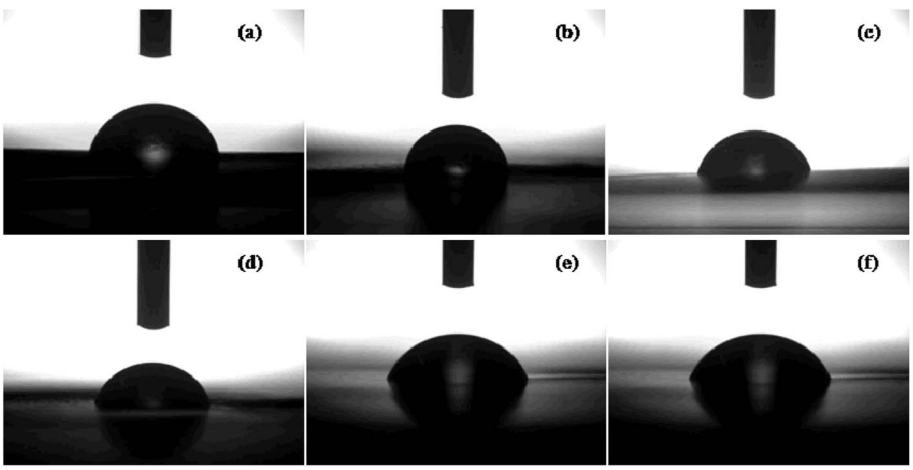

Fig. 3 Image of droplets formed on the surface of (a) PLA/PBAT blend control film, (b) PLA/PBAT blend + 1 wt% ε-PL film, (c) PLA/PBAT blend + 2 wt% ε-PL film, (d) PLA/PBAT blend + 3 wt% ε-PL film, (e) PLA/PBAT blend + 4 wt% ε-PL film, and (f) PLA/PBAT blend + 5 wt% ε-PL film.

irregularities due to its limited compatibility and dispersion within the polymer blend.

3.3. Contact angle measurement

The primary function of contact angle measurement is to evaluate a solid surface's wettability by a liquid, providing essential information regarding its hydrophilicity or hydrophobicity. Surfaces with contact angles below 90° are considered hydrophilic, as they promote liquid spreading and exhibit high wettability. Conversely, contact angles above 90° denote hydrophobic surfaces, where liquids tend to bead up due to low wettability. In this study, the contact angle data for PLA/PBAT blend control films and those loaded with different weight percentages of ε-PL (1–5 wt%) are presented in Table 1, with corresponding droplet images shown in Fig. 3. The control PLA/PBAT blend film exhibited a contact angle of 72.23°, indicating a moderately hydrophobic surface.[32] As the ε-PL concentration varied from 1 to 5 wt%, a consistent decrease in the contact angle was observed, ultimately resulting in a value of 47.43°. This steady reduction in the contact angle reflects a progressive increase in surface hydrophilicity. The cationic, hydrophilic polypeptide ε-PL contains abundant amino groups that readily form hydrogen bonds with H_2O molecules, thereby improving wettability and lowering the contact angle when incorporated into the polymer matrix. Similar improvements in hydrophilicity have been reported in studies where ε-PL was grafted onto membranes.[33] Overall, these findings demonstrate that the addition of ε-PL significantly improves the hydrophilicity of the blend films.

3.4. DSC analysis

DSC was employed to investigate the effect of ε-PL on the thermal characteristics of PLA/PBAT blend films, specifically their T_m, T_g and T_c. The incorporation of ε-PL led to the reduction of the T_g of PLA from 47.88 °C to 44.33 °C (Fig. 4). This reduction is attributed to interactions between ε-PL and PLA *via* hydrogen bonding or ionic interactions, which disrupt the regular arrangement of PLA chains and enhanced chain mobility, effectively acting as a secondary plasticizer.[34] The T_g continued to decrease with increasing ε-PL content, reaching a minimum at 4 wt% (43.21 °C), but then slightly increased at 5 wt% (44.21 °C). This shows that the plasticizing effect of ε-PL might have diminished beyond a certain concentration. Cold crystallization, a phenomenon where polymer crystallization occurs during heating rather than cooling, was observed at 103.89 °C, suggesting that PLA was not fully crystallized—possibly due to rapid cooling.[35]

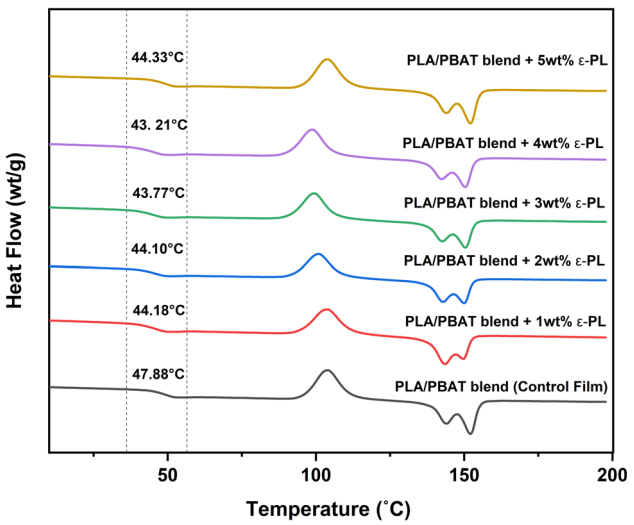

Fig. 4 DSC thermogram of the PLA/PBAT blend control film and PLA/PBAT blend films loaded with different weight percentages of ε-PL (1–5 wt%).

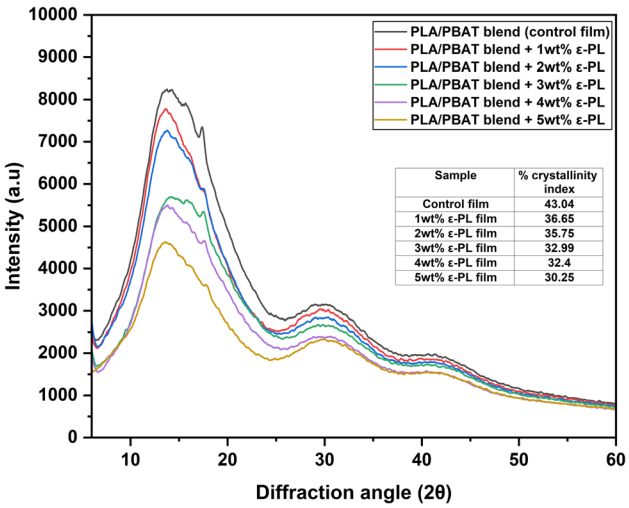

Fig. 5 XRD graph of the PLA/PBAT blend control film and PLA/PBAT blend loaded films with different weight percentages of ε-PL (1–5 wt%).

The DSC thermograms revealed a split melting peak: a lower melting peak (T_m1) between 140 and 145 °C (corresponding to less perfect crystals formed during cold crystallization) and a higher melting peak (T_m2) between 145 and 150 °C (resulting from well-arranged crystals formed subsequently).[36] With increasing ε-PL content, cold crystallization initially decreased, indicating enhanced chain mobility and flexibility that allowed for crystal rearrangement at lower temperatures. However, this trend reversed at ε-PL concentrations above 4 wt%, as cold crystallization increased with further ε-PL addition. These results provide valuable insights into the thermal behavior and structural dynamics of these polymer blends.

3.5. XRD analysis

XRD was employed to investigate the effect of ε-PL on the crystallinity of PLA/PBAT blend films. Fig. 5 presents the XRD patterns of the PLA/PBAT blend film and those with ε-PL incorporated at 1–5 wt%. The PLA/PBAT blend film exhibits a distinct diffraction peak at $2\theta \approx 17.45°$, corresponding to the (200)/(110) reflections of the α-form of PLA, confirming its semi-crystalline nature.[37] An increase in ε-PL content from 1 to 5 wt% results in broadening of the XRD peak, reflecting a progressive

Table 2 Thickness and OTR values of PLA/PBAT blend control films and PLA/PBAT blend loaded films with different weight percentages of ε-PL (1–5 wt%)[a]

Sample	Thickness (μm)	OTR ($cm^3\ m^{-2}\ d^{-1}$)
PLA/PBAT blend control film	65.84 ± 1.46^{a}	317.00 ± 4.35^{a}
PLA/PBAT blend + 1 wt% ε-PL	65.46 ± 1.45^{a}	368.47 ± 1.88^{b}
PLA/PBAT blend + 2 wt% ε-PL	67.69 ± 2.42^{a}	374.24 ± 3.90^{bc}
PLA/PBAT blend + 3 wt% ε-PL	65.41 ± 1.49^{a}	384.21 ± 4.31^{cd}
PLA/PBAT blend + 4 wt% ε-PL	67.20 ± 1.62^{a}	394.56 ± 4.45^{de}
PLA/PBAT blend + 5 wt% ε-PL	68.05 ± 1.60^{a}	404.86 ± 4.51^{e}

[a] Values in the same column with different lowercase letters (a–e) are significantly different at $p \leq 0.05$. All values are expressed as the mean ± SD ($n = 3$).

reduction in crystallinity and a shift toward an amorphous phase. At 5 wt% ε-PL, the blend film displays an amorphous halo, signifying a predominantly amorphous state. This may be attributed to the amorphous and hydrophilic nature of ε-PL, which likely interacts with PLA through hydrogen bonding or ionic interactions, thereby increasing chain mobility and disrupting the regular arrangement of PLA chains, ultimately reducing crystallinity.[38] These results indicate that ε-PL is not merely physically mixed within the polymer matrix, but rather forms a more complex association with the blend, suggesting interactions at the molecular level.

3.6. Assessment of barrier performance

The oxygen and moisture barrier characteristics of the films were assessed, and the results are presented in Tables 2 and 3 respectively. The addition of ε-PL into the PLA/PBAT matrix increases the OTR values, due to the hydrophilic nature of ε-PL, which introduces more polar sites into the originally dense polymer matrix. The incorporation of ε-PL disrupts the regular packing of molecular chains within the PLA/PBAT matrix, resulting in a more loosely packed structure with increased chain mobility and excess free volume compared to the original films. This disruption reduces crystallinity, as confirmed by XRD analysis. The increased chain mobility and excess free volume, resulting from this de-densification effect,[39] facilitate greater oxygen permeability. Similarly, WVTR progressively increases with ε-PL content (1 to 5 wt%). This trend is attributed to the polar amino groups in ε-PL, which increases moisture permeability by introducing hydrophilic sites within the film.[40] These modifications improve gas and moisture exchange and increase both the OTR and WVTR. This enhanced permeability supports improved respiration dynamics, moisture balance and adequate gas exchange for packaged fruits and vegetables, thereby extending their shelf life.

Table 3 Thickness and WVTR values of PLA/PBAT blend control films and PLA/PBAT blend loaded films with different weight percentages of ε-PL (1–5 wt%)[a]

Sample	Thickness (μm)	WVTR ($g\ m^{-2}\ d^{-1}$)
PLA/PBAT blend control film	65.18 ± 1.00^{a}	417.00 ± 4.36^{a}
PLA/PBAT blend + 1 wt% ε-PL	67.69 ± 1.62^{a}	468.80 ± 1.35^{b}
PLA/PBAT blend + 2 wt% ε-PL	66.87 ± 1.08^{a}	477.58 ± 2.50^{bc}
PLA/PBAT blend + 3 wt% ε-PL	68.39 ± 1.97^{a}	483.54 ± 4.37^{c}
PLA/PBAT blend + 4 wt% ε-PL	66.08 ± 1.80^{a}	500.90 ± 3.64^{d}
PLA/PBAT blend + 5 wt% ε-PL	66.13 ± 1.01^{a}	515.53 ± 4.50^{e}

[a] Values in the same column with different lowercase letters (a–e) are significantly different at $p \leq 0.05$. All values are expressed as the mean ± SD ($n = 3$).

3.7. Mechanical properties

Incorporating hydrophilic additives such as ε-PL into PLA/PBAT blend films results in notable changes to the mechanical properties, as evaluated across different weight percentages (1–5 wt%) of ε-PL. These results, detailed in Table 4 and illustrated in the stress–strain graph (Fig. 6), highlight the impact of ε-PL content on several mechanical properties. The PLA/PBAT film without ε-PL possesses a tensile strength of 31.22 MPa. The addition of ε-PL resulted in a steady decline in tensile strength to 26.14 MPa, primarily due to its plasticizing effect that enhances the polymer chain mobility and reduces the overall rigidity. This trend is mirrored in the Young's modulus, which dropped from 2019.86 MPa to 1559.9 MPa as the ε-PL concentration increased from 1 to 5 wt%, indicating increased film flexibility and decreased stiffness. Elongation at break for the control film was 33.94%, but this value increased gradually with ε-PL content up to 4 wt%, reaching between 44.82% and 65.47%, consistent with a plasticizing effect at moderate concentrations.[41] However, at 5 wt% ε-PL, elongation dropped to 55.47%, suggesting the formation of weak regions within the matrix at higher additive levels. These findings highlight the optimal performance observed at intermediate concentrations. These results are relevant for designing biodegradable active

Table 4 Mechanical properties of PLA/PBAT blend control films and PLA/PBAT blend loaded films with different weight percentages of ε-PL (1–5 wt%)[a]

Sample	Tensile strength (MPa)	Young's modulus (MPa)	% Elongation
PLA/PBAT blend control film	31.22 ± 3.63^{c}	2019.86 ± 50.07^{d}	33.94 ± 0.57^{a}
PLA/PBAT blend + 1 wt% ε-PL	30.19 ± 0.81^{bc}	1939.92 ± 43.35^{d}	44.82 ± 2.71^{b}
PLA/PBAT blend + 2 wt% ε-PL	28.77 ± 0.74^{abc}	1802.78 ± 44.11^{c}	46.01 ± 1.98^{b}
PLA/PBAT blend + 3 wt% ε-PL	27.92 ± 1.03^{abc}	1729.1 ± 59.65^{bc}	50.87 ± 1.50^{c}
PLA/PBAT blend + 4 wt% ε-PL	27.10 ± 1.04^{ab}	1654.01 ± 37.87^{b}	65.47 ± 2.54^{e}
PLA/PBAT blend + 5 wt% ε-PL	26.14 ± 1.01^{a}	1559.9 ± 42.59^{a}	55.47 ± 3.55^{d}

[a] Values in the same column with different lowercase letters (a–e) are significantly different at $p \leq 0.05$. All values are expressed as the mean ± SD ($n = 5$).

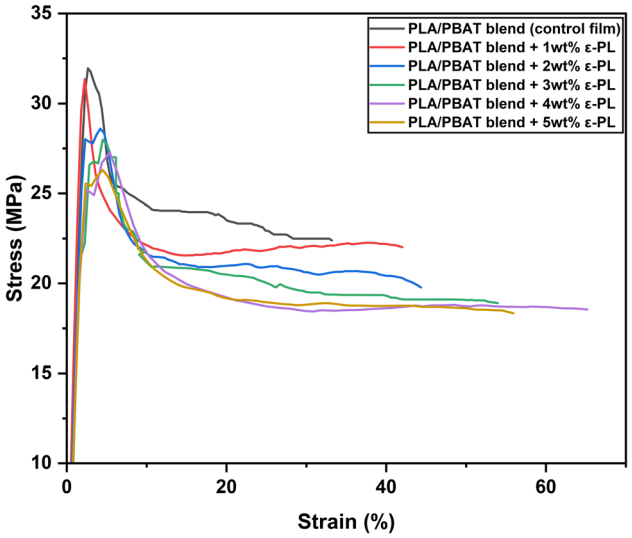

Fig. 6 Stress–strain curve of the PLA/PBAT blend control film and PLA/PBAT blend films loaded with different weight percentages of ε-PL (1–5 wt%).

packaging, especially when balancing mechanical integrity with the need for flexibility and elongation properties for food applications.

3.8. Antimicrobial property evaluation

ε-PL shows effective antibacterial activity against a wide range of Gram-negative and Gram-positive bacterial strains. Initially, cationic ε-PL interacts electrostatically with the negatively charged phospholipids of the bacterial membrane, resulting in membrane disruption. This process is commonly described as a "carpet-like" mechanism, where ε-PL molecules cover and disrupt the membrane surface. In Gram-negative bacteria, ε-PL destabilizes the lipopolysaccharide layer, while in Gram-positive bacteria, it targets the peptidoglycan layer. These interactions induce negative membrane curvature, resulting in the formation of micelles and pores that compromise membrane integrity and increase permeability, ultimately causing bacterial lysis and cell death.[42] The well diffusion assay quantified antibacterial activity of PLA/PBAT blend films containing various concentrations of ε-PL against *E. coli* and *S. aureus*. The inhibition zone measurements obtained through this method quantitatively reflect the antimicrobial effectiveness corresponding to different ε-PL concentrations. The results (Fig. 7) demonstrate a clear concentration-dependent increase in antimicrobial efficacy with higher ε-PL content. Specifically, at 1 wt% ε-PL, the zones of inhibition measured 20.6 mm for *E. coli* and 25.3 mm for *S. aureus*. These zones expanded to 27.3 mm and 30.6 mm, respectively, at 5 wt% ε-PL, indicating a progressive enhancement of antibacterial activity as ε-PL concentration increases. The greater inhibitory effect observed against *S. aureus* compared to *E. coli* suggests that ε-PL is more effective against Gram-positive bacteria. This variation is due to distinct structural features of the bacterial cell walls: Gram-positive organisms such as *S. aureus* have a thick peptidoglycan layer but lack an outer membrane, making them more vulnerable to antimicrobial agents. In contrast, Gram-negative bacteria like *E. coli* have a thinner peptidoglycan layer but are protected by an additional outer membrane, which hinders the penetration of antimicrobial compounds.[43] These findings confirm the potential of natural antimicrobial additives like ε-PL in active packaging systems, promoting enhanced food safety and environmental sustainability.

3.9. Release kinetics of the antimicrobial agent

The release kinetics of ε-PL from PLA/PBAT blend films, loaded with 1–5 wt% ε-PL, were analyzed by fitting experimental data to several established models such as the Higuchi, Korsmeyer–Peppas, first-order and zero-order models. The experimental

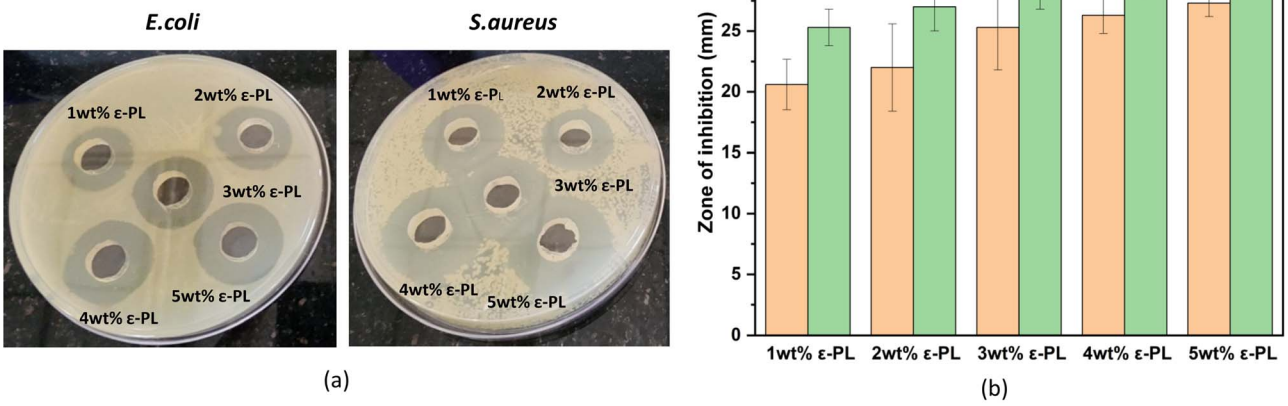

Fig. 7 (a) Antimicrobial activity of PLA/PBAT blend films loaded with different weight percentages of ε-PL (1–5 wt%) using film extract (200 μL) evaluated by the well diffusion assay and incubated at 37 °C for 24 h. (b) Zone of inhibition bar graph of PLA/PBAT with ε-PL (1–5 wt%) film extract against *E. coli* and *S. aureus*.

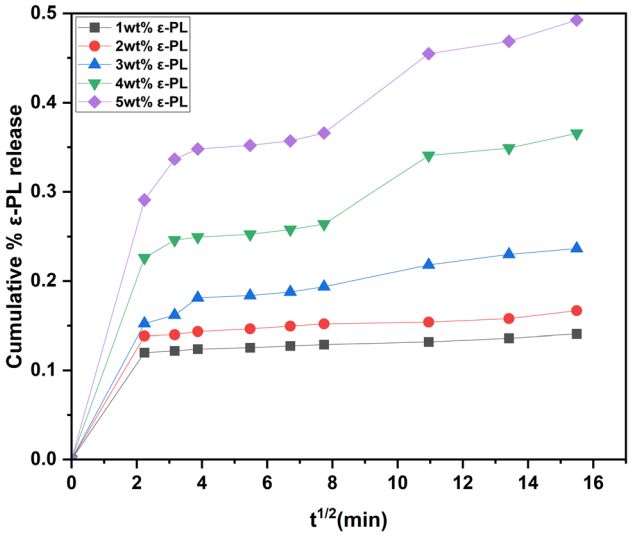

Fig. 8 ε-PL release curve of PLA/PBAT blend films loaded with different weight percentages of ε-PL (1–5 wt%).

data moderately fit the zero-order model, indicating a roughly constant release rate independent of concentration, which suggests that the system does not facilitate uniform release. The first-order model, which assumes release proportional to the remaining ε-PL concentration, did not fit well, as ε-PL is physically entrapped in the polymer matrix and no significant concentration-dependent decay was observed. The Korsmeyer–Peppas model, typically used to describe initial drug release from polymeric matrices (up to 60% release, $Mt/M\infty < 0.6$),[44] was deemed invalid in this case because the release exceeded this threshold ($Mt/M\infty > 0.6$). Among the evaluated models, the Higuchi model provided the best fit, with high R^2 values ranging from 0.96 to 0.98. This model describes release as a diffusion-controlled process, which is characteristic of systems where the active agent is dispersed in an insoluble polymer matrix and diffuses out into the surrounding medium.[45] A plot of cumulative ε-PL release *versus* the square root of time was generated, and its linearity (Fig. 8) indicated that Fickian diffusion through the polymer matrix is the dominant release mechanism. This diffusion-driven release is especially beneficial for active food packaging, as it enables sustained antibacterial activity throughout the storage period.

3.10. Shelf life studies of bananas packed in antimicrobial films

The quality parameters of bananas packed in PLA/PBAT blend films incorporated with ε-PL were compared with those of bananas packed in control films and unpacked banana samples. Fig. 9 demonstrates the gradual quality changes during 7 days of storage, with bananas in ε-PL films exhibiting superior shelf life compared to both bananas packed in control films and unpacked fruit. This is supported by Fig. 10(a), which illustrates that unpacked bananas experienced the highest weight loss (33.7%), while those in control and ε-PL films showed significantly lower weight loss (11.5% and 9.0%, respectively). These findings align with earlier research involving PLA/PBAT/TPS films with salicylic acid and MCM-41, which similarly reduced weight loss and extended banana shelf life.[46]

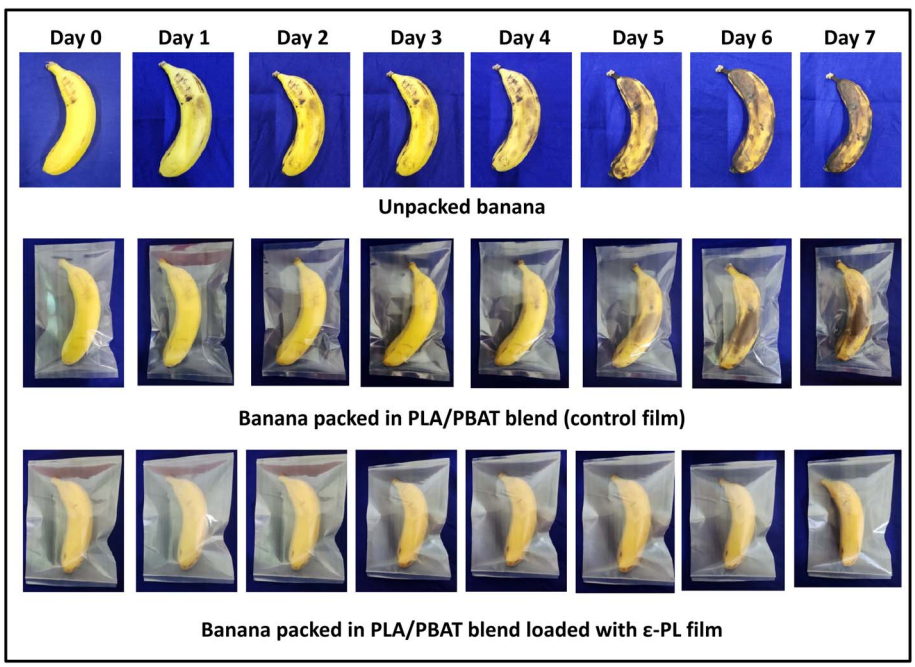

Fig. 9 Images showing the quality deterioration of bananas during 7 days of storage.

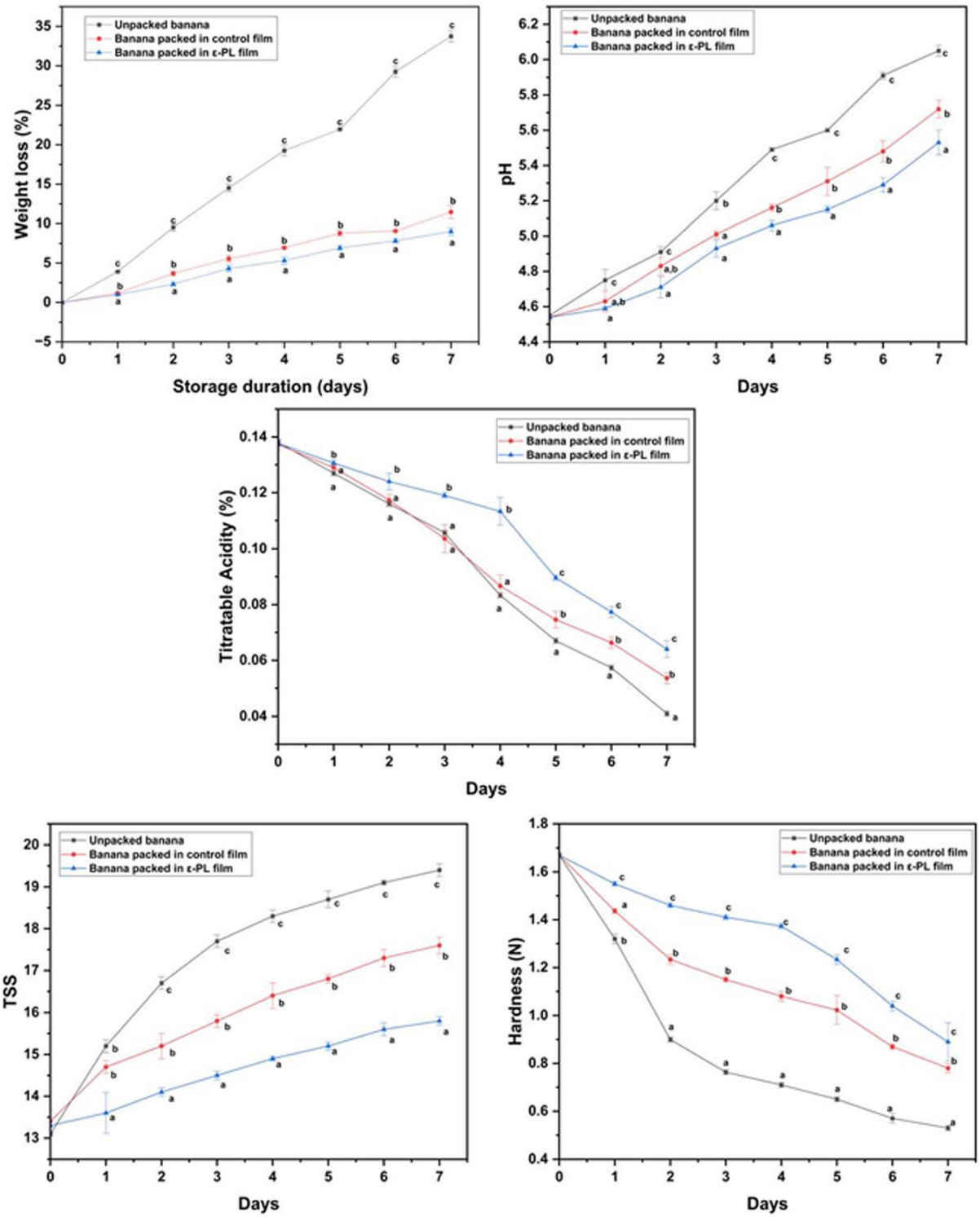

Fig. 10 Changes in the physicochemical characteristics of bananas (percentage weight loss, pH, titratable acidity, TSS, and hardness) during 7 days of storage at room temperature under three packaging conditions: unpacked, packed in PLA//PABT blend control films and PLA/PBAT blend films loaded with 4 wt% ε-PL. Values in the same column with different lowercase letters (a–c) are significantly different at $p \leq 0.05$. All values are expressed as the mean ± SD ($n = 3$).

Hardness, a key indicator of banana texture, steadily decreased in unpacked bananas (from 1.67 N to 0.53 N), whereas bananas in ε-PL films retained higher hardness for a longer duration (from 1.67 N to 0.78 N). Control film-packaged bananas showed intermediate hardness loss. This indicates that ε-PL not only inhibits microbial growth but also helps

Table 5 L^*, a^*, and b^* color parameters of bananas during 7 days of storage[a]

Days	Unpacked bananas (L^*)	Bananas packed in control films (L^*)	Bananas packed in ε-PL films (L^*)	Unpacked bananas (a^*)	Bananas packed in control films (a^*)	Bananas packed in ε-PL films (a^*)	Unpacked bananas (b^*)	Bananas packed in control films (b^*)	Bananas packed in ε-PL films (b^*)
0	72.92 ± 0.73^{l}	72.75 ± 0.44^{l}	72.58 ± 1.17^{l}	1.05 ± 0.04^{a}	1.07 ± 0.01^{a}	1.07 ± 0.01^{a}	24.93 ± 0.67^{a}	24.93 ± 0.67^{a}	24.96 ± 0.47^{a}
1	67.44 ± 0.37^{j}	68.11 ± 0.18^{j}	70.99 ± 0.24^{k}	1.47 ± 0.02^{d}	1.24 ± 0.01^{b}	1.13 ± 0.02^{a}	30.82 ± 1.21^{def}	29.64 ± 0.52^{cd}	27.38 ± 0.16^{b}
2	64.27 ± 0.16^{h}	66.34 ± 0.16^{i}	68.51 ± 0.41^{j}	1.6 ± 0.02^{e}	1.46 ± 0.03^{d}	1.22 ± 0.02^{b}	33.58 ± 0.43^{hi}	31.37 ± 0.06^{efg}	29.37 ± 0.09^{c}
3	62.40 ± 0.48^{fg}	64.89 ± 0.07^{h}	65.16 ± 0.04^{h}	1.70 ± 0.02^{f}	1.48 ± 0.01^{d}	1.37 ± 0.01^{c}	35.84 ± 0.11^{j}	32.03 ± 0.04^{fg}	30.65 ± 0.55^{de}
4	60.25 ± 0.1^{d}	62.59 ± 0.11^{fg}	64.85 ± 0.14^{h}	1.97 ± 0.01^{hi}	1.73 ± 0.02^{f}	1.50 ± 0.01^{d}	37.49 ± 0.19^{k}	35.84 ± 0.02^{j}	32.53 ± 0.06^{gh}
5	59.04 ± 0.03^{b}	61.09 ± 0.03^{de}	62.87 ± 0.06^{g}	2.02 ± 0.01^{i}	1.84 ± 0.02^{g}	1.68 ± 0.01^{ef}	38.04 ± 0.03^{kl}	36.06 ± 0.02^{j}	34.39 ± 0.45^{i}
6	58.8 ± 0.1^{b}	60.15 ± 0.05^{cd}	61.64 ± 0.09^{ef}	2.21 ± 0.02^{k}	1.93 ± 0.02^{h}	1.83 ± 0.02^{g}	39.01 ± 0.01^{lm}	37.4 ± 0.1^{k}	35.7 ± 0.1^{j}
7	57.47 ± 0.06^{a}	59.09 ± 0.01^{bc}	60.17 ± 0.11^{d}	2.47 ± 0.01^{l}	2.1 ± 0.09^{j}	1.93 ± 0.02^{h}	39.39 ± 0.03^{m}	38.1 ± 0.09^{kl}	36.01 ± 0.01^{j}

[a] Values in the same column with different lowercase letters (a–m) are significantly different at $p \leq 0.05$. All values are expressed as the mean ± SD ($n = 3$).

maintain fruit texture by slowing ripening and softening. These results are consistent with previous studies on active and passive modified atmosphere packaging, where active packaging strategies effectively delayed textural changes and preserved banana quality.[47]

Table 5 demonstrates changes in banana color parameters (L^*, a^*, and b^*) during storage. L^* (lightness) decreases for all samples due to browning, but bananas in ε-PL films show a slower decline (L^*: 72.5 to 60.17) compared to unpacked fruit (L^*: 72.9 to 57.47), indicating better visual quality preservation. All samples shift toward redder (a^*) and yellower (b^*) hues with storage, reflecting ripening and enzymatic browning. However, ε-PL films delay these color changes compared to unpacked and control-packaged bananas, suggesting superior protection against visual degradation. Physicochemical analysis confirms this trend.[48] The pH of bananas increases with storage, while TA decreases, indicating reduced acid content. TSS also increase, with unpacked bananas showing the highest TSS (19.4° brix), followed by control (17.6° brix) and ε-PL films (15.8° brix), demonstrating delayed ripening in the latter. Thus PLA/PBAT films loaded with ε-PL significantly slow down color changes, ripening, and quality deterioration in bananas. The observed improvements in banana quality were statistically analyzed using IBM SPSS version 20.0 (SPSS Inc., Chicago, IL). One-way ANOVA was performed to evaluate differences among groups, followed by Tukey's *post hoc* test to identify significant pairwise comparisons at $p \leq 0.05$. The findings were consistent with previous studies on banana ripening under various packaging conditions.[49]

4 Conclusions

Blown film extrusion was used to fabricate PLA/PBAT blend films containing varying concentrations of ε-PL, and the presence of ε-PL in the films was confirmed by FTIR analysis. Comprehensive studies revealed that increasing ε-PL content enhances film hydrophilicity (confirmed by contact angle measurements) and decreases crystallinity (*via* XRD and DSC), and barrier properties were affected due to the hydrophilic nature of ε-PL. SEM analysis verified that loading ε-PL in the PLA/PBAT blend film increased its surface roughness while also improving surface wettability. Mechanical testing showed that elongation at break increases up to 4 wt% ε-PL, after which it declines, indicating optimal mechanical performance at this concentration. Antimicrobial evaluations demonstrated potent activity, with 5 wt% ε-PL films exhibiting significant inhibition zones against *Staphylococcus aureus* and *Escherichia coli*, highlighting ε-PL's broad-spectrum efficacy. Release kinetics studies, analyzed using the Higuchi model, revealed that ε-PL release follows Fickian diffusion, ensuring a regulated and sustained release from the polymer matrix. This controlled release is advantageous for maintaining antimicrobial activity throughout the storage period. Bananas packaged in ε-PL-loaded films showed superior resistance to quality deterioration—including reduced browning, slower ripening, and better retention of firmness—compared to those in control films and unpacked samples. Overall, PLA/PBAT films loaded with ε-PL represent a promising, sustainable solution for active food

packaging, effectively extending shelf life, ensuring food safety, and reducing reliance on petrochemical based plastic films.

Author contributions

Smrithy Pullarkad Bharathan: writing original draft, investigation, methodology, writing. Johnsy George: conceptualisation, methodology, supervision, writing – review & editing. Aksalamol Pallivathukkal Raju: investigation, methodology. Mahammad Riyaz Guthige: investigation, methodology. Chandrika Gowdahalli Mantelingachar: investigation, methodology. Venugopal Vasudevan: formal analysis. Radhika Madan Urs: investigation, methodology. Ranganathan Kumar: supervision, overall monitoring.

Conflicts of interest

The authors have no competing interests to declare.

Data availability

All necessary data to substantiate this article are contained within the text, with any further information available upon request.

Supplementary information: thermogravimetric analysis (TGA) curve of ε-PL and correlation coefficients (R^2) of Higuchi, first-order, and zero-order kinetic models. See DOI: **https://doi.org/10.1039/d5fb00286a**.

Acknowledgements

DRDO. The authors express their sincere gratitude to the Centre Head, DIBT, Mysore, for his continuous support and encouragement.

References

1 M. E. González-López, S. D. Calva-Estrada, M. S. Gradilla-Hernández and P. Barajas-Álvarez, Current trends in biopolymers for food packaging: a review, *Front. Sustain. Food Syst.*, 2023, **7**, 1225371.
2 K. Y. Perera, A. K. Jaiswal and S. Jaiswal, Biopolymer-based sustainable food packaging materials: challenges, solutions, and applications, *Foods*, 2023, **12**(12), 2422.
3 J. George, S. N. Sabapathi, Siddaramaiah, Water soluble polymer-based nanocomposites containing cellulose nanocrystals, *Eco-friendly polymer nanocomposites: processing and properties*, 2015, pp. 259–293.
4 C. Sudheesh, K. V. Sunooj, V. Jamsheer, S. Sabu, A. Sasidharan, B. Aaliya, M. Navaf, P. P. Akhila and J. George, Development of bioplastic films from γ^- irradiated kithul (*Caryota urens*) starch; morphological, crystalline, barrier, and mechanical characterization, *Starch/Staerke*, 2021, **73**(5–6), 2000135.
5 L. Shao, Y. Xi and Y. Weng, Recent advances in PLA-based antibacterial food packaging and its applications, *Molecules*, 2022, **27**(18), 5953.
6 E. Sritham, P. Phunsombat and J. Chaishome, Tensile properties of PLA/PBAT blends and PLA fibre-reinforced PBAT composite, in *MATEC Web of Conferences*, EDP Sciences, 2018, vol. 192, p. 03014.
7 J. R. Westlake, M. W. Tran, Y. Jiang, X. Zhang, A. D. Burrows and M. Xie, Biodegradable active packaging with controlled release: principles, progress, and prospects, *ACS Food Sci. Technol.*, 2022, **2**(8), 1166–1183.
8 V. Suvarna, A. Nair, R. Mallya, T. Khan and A. Omri, Antimicrobial nanomaterials for food packaging, *Antibiotics*, 2022, **11**(6), 729.
9 C. Tan, F. Han, S. Zhang, P. Li and N. Shang, Novel bio-based materials and applications in antimicrobial food packaging: recent advances and future trends, *Int. J. Mol. Sci.*, 2021, **22**(18), 9663.
10 M. Hyldgaard, T. Mygind, B. S. Vad, M. Stenvang, D. E. Otzen and R. L. Meyer, The antimicrobial mechanism of action of epsilon-poly-L-lysine, *Appl. Environ. Microbiol.*, 2014, **80**(24), 7758–7770.
11 B. Rodrigues, T. P. Morais, P. A. Zaini, C. S. Campos, H. O. Almeida-Souza, A. M. Dandekar, R. Nascimento and L. R. Goulart, Antimicrobial activity of epsilon-poly-L-lysine against phytopathogenic bacteria, *Sci. Rep.*, 2020, **10**(1), 11324.
12 J. N. Liu, S. L. Chang, P. W. Xu, M. H. Tan, B. Zhao, X. D. Wang and Q. S. Zhao, Structural changes and antibacterial activity of epsilon-poly-L-lysine in response to pH and phase transition and their mechanisms, *J. Agric. Food Chem.*, 2020, **68**(4), 1101–1109.
13 Y. Chen, W. Miao, X. Li, Y. Xu, H. Gao and B. Zheng, The structure, properties, synthesis method and antimicrobial mechanism of ε-polylysine with the preservative effects for aquatic products, *Trends Food Sci. Technol.*, 2023, **139**, 104131.
14 E. Lebaudy, C. Guilbaud-Chéreau, B. Frisch, N. E. Vrana and P. Lavalle, The High Potential of ε-Poly-L-Lysine for the Development of Antimicrobial Biomaterials, *Adv. NanoBiomed Res.*, 2023, **3**(12), 2300080.
15 Z. Mousavi, M. Naseri, S. Babaei, S. M. Hosseini and S. S. Shekarforoush, The effect of cross-linker type on structural, antimicrobial and controlled release properties of fish gelatin-chitosan composite films incorporated with ε-poly-L-lysine, *Int. J. Biol. Macromol.*, 2021, **183**, 1743–1752.
16 R. Bao, X. He, Y. Liu, Y. Meng and J. Chen, Preparation, characterization, and application of sodium alginate/ε-polylysine layer-by-layer self-assembled edible film, *Coatings*, 2023, **13**(3), 516.
17 H. Yang, Q. Li, L. Yang, T. Sun, X. Li, B. Zhou and J. Li, The competitive release kinetics and synergistic antibacterial characteristics of tea polyphenols/ε-poly-L-lysine hydrochloride core–shell microcapsules against *Shewanella putrefaciens*, *Int. J. Food Sci. Technol.*, 2020, **55**(12), 3542–3552.
18 P. R. Aksalamol, J. George, M. R. Guthige, M. Navaf, K. V. Sunooj, R. Kumar and A. D. Semwal, Towards sustainable food packaging: optimization of suitable

sorbitan surfactant for the development of PLA-based antifog film, *Food Packag. Shelf Life*, 2024, **46**, 101368.
19 J. George, R. Kumar, C. Jayaprahash, A. Ramakrishna, S. N. Sabapathy and A. S. Bawa, Rice bran-filled biodegradable low-density polyethylene films: development and characterization for packaging applications, *J. Appl. Polym. Sci.*, 2006, **102**(5), 4514–4522.
20 J. George, S. G. Nair, R. Kumar, A. D. Semwal, C. Sudheesh, A. Basheer and K. V. Sunooj, A new insight into the effect of starch nanocrystals in the retrogradation properties of starch, *Food Hydrocolloids Health*, 2021, **1**, 100009.
21 S. Chowdhury, Y. L. Teoh, K. M. Ong, N. S. Zaidi and S. K. Mah, Poly(vinyl)alcohol crosslinked composite packaging film containing gold nanoparticles on shelf life extension of banana, *Food Packag. Shelf Life*, 2020, **24**, 100463.
22 L. Stagi, M. Sini, D. Carboni, R. Anedda, G. Siligardi, T. M. Gianga, R. Hussain and P. Innocenzi, Modulating the poly-L-lysine structure through the control of the protonation–deprotonation state of L-lysine, *Sci. Rep.*, 2022, **12**(1), 19719.
23 P. Cunniff and D. Washington, Official methods of analysis of AOAC International, *J. AOAC Int.*, 1997, **80**(6), 127A.
24 X. Ma, Y. Wang, J. Wang and Y. Xu, Effect of PBAT on property of PLA/PHB film used for fruits and vegetables, in *MATEC Web of Conferences*, EDP Sciences, 2017, vol. 88, p. 02009.
25 E. Sritham, P. Phunsombat and J. Chaishome, Tensile properties of PLA/PBAT blends and PLA fibre-reinforced PBAT composite, in *MATEC Web of Conferences*, EDP Sciences, 2018, vol. 192, p. 03014.
26 J. Wu, L. Wang and B. Qi, Effects of Chitosan Nanoparticles and 4,4′-Methylene-Diphenyl Diisocyanate on the Polylactic Acid/Poly(Butyleneadipate-*co*-Terephthalate) Composite Properties, *Membranes*, 2023, **13**(7), 637.
27 L. Jiang, B. Liu and J. Zhang, Properties of poly(lactic acid)/poly(butylene adipate-*co*-terephthalate)/nanoparticle ternary composites, *Ind. Eng. Chem. Res.*, 2009, **48**(16), 7594–7602.
28 J. V. Azevedo, E. Ramakers-van Dorp, R. Grimmig, B. Hausnerova and B. Möginger, Process-induced morphology of poly(butylene adipate terephthalate)/poly(lactic acid) blown extrusion films modified with chain-extending cross-linkers, *Polymers*, 2022, **14**(10), 1939.
29 A. Kassem, L. Abbas, O. Coutinho, S. Opara, H. Najaf, D. Kasperek, K. Pokhrel, X. Li and S. Tiquia-Arashiro, Applications of Fourier Transform-Infrared spectroscopy in microbial cell biology and environmental microbiology: advances, challenges, and future perspectives, *Front. Microbiol.*, 2023, **14**, 1304081.
30 M. Nochi, Y. Ozaki and H. Sato, Water-induced conformational changes in the powder and film of ε-poly(L) lysine studied by infrared and Raman spectroscopy, *Spectrochim. Acta, Part A*, 2021, **260**, 119900.
31 Z. N. Correa-Pacheco, J. D. Black-Solís, P. Ortega-Gudiño, M. A. Sabino-Gutiérrez, J. J. Benítez-Jiménez, A. Barajas-Cervantes, S. Bautista-Baños and L. B. Hurtado-Colmenares, Preparation and characterization of bio-based PLA/PBAT and cinnamon essential oil polymer fibers and life-cycle assessment from hydrolytic degradation, *Polymers*, 2019, **12**(1), 38.
32 M. Y. Ghadhban, K. T. Rashid, A. A. Abdulrazak, I. T. Ibrahim, Q. F. Alsalhy, Z. M. Shakor and I. Hamawand, Modification of Polylactide-poly(butylene adipate-co-terephthalate)(PLA/PBAT) Mixed-Matrix Membranes (MMMs) with Green Banana Peel Additives for Oil Wastewater Treatment, *Water*, 2024, **16**(7), 1040.
33 M. Yan, M. Shao, J. Li, N. Jiang, Y. Hu, W. Zeng and M. Huang, Antifouling forward osmosis membranes by ε-polylysine mediated molecular grafting for printing and dyeing wastewater: preparation, characterization, and performance, *J. Membr. Sci.*, 2023, **668**, 121288.
34 Y. Wang, L. Huang, Y. Shen, L. Tang, R. Sun, D. Shi, T. J. Webster, J. Tu and C. Sun, Electrostatic interactions between polyglutamic acid and polylysine yields stable polyion complex micelles for deoxypodophyllotoxin delivery, *Int. J. Nanomed.*, 2017, **30**, 7963–7977.
35 N. D. Bikiaris, P. A. Klonos, E. Christodoulou, P. Barmpalexis and A. Kyritsis, Plasticization Effects of PEG of Low Molar Fraction and Molar Mass on the Molecular Dynamics and Crystallization of PLA-b-PEG-b-PLA Triblock Copolymers Envisaged for Medical Applications, *J. Phys. Chem. B*, 2025, **129**(13), 3514–3528.
36 Z. F. Bai and Q. Dou, Melting and crystallization behaviors of poly(lactic acid)/polypropylene blends, in *2015 International Conference on Material Science and Applications (icmsa-15)*, Atlantis Press, 2014, pp. 282–286.
37 M. Giełdowska, M. Puchalski, S. Sztajnowski and I. Krucińska, Evolution of the molecular and supramolecular structures of PLA during the thermally supported hydrolytic degradation of wet spinning fibers, *Macromolecules*, 2022, **55**(22), 10100–10112.
38 R. Y. Zhang, P. F. Wang, H. X. Li, Y. J. Yang and S. Q. Rao, Enhanced Antibacterial Efficiency and Anti-Hygroscopicity of Gum Arabic–ε-Polylysine Electrostatic Complexes: Effects of Thermal Induction, *Polymers*, 2023, **15**(23), 4517.
39 S. Marano, E. Laudadio, C. Minnelli and P. Stipa, Tailoring the barrier properties of PLA: a state-of-the-art review for food packaging applications, *Polymers*, 2022, **14**(8), 1626.
40 Z. Yu, D. Gong, C. Han, Y. Wei, C. Fu, X. Xu and Y. Lu, Preparation and properties of pea starch/ε-polylysine composite films, *Materials*, 2022, **15**(6), 2327.
41 X. Tang and S. Alavi, Recent advances in starch, polyvinyl alcohol based polymer blends, nanocomposites and their biodegradability, *Carbohydr. Polym.*, 2011, **85**(1), 7–16.
42 M. Hyldgaard, T. Mygind, B. S. Vad, M. Stenvang, D. E. Otzen and R. L. Meyer, The antimicrobial mechanism of action of epsilon-poly-L-lysine, *Appl. Environ. Microbiol.*, 2014, **80**(24), 7758–7770.
43 A. H. Delcour, Outer membrane permeability and antibiotic resistance, *Biochim. Biophys. Acta, Proteins Proteomics*, 2009, **1794**(5), 808–816.
44 R. Scaffaro, A. Maio, F. E. Gulino, C. Di Salvo and A. Arcarisi, Bilayer biodegradable films prepared by co-extrusion film

blowing: mechanical performance, release kinetics of an antimicrobial agent and hydrolytic degradation, *Composites, Part A*, 2020, **132**, 105836.

45 D. R. Paul, Elaborations on the Higuchi model for drug delivery, *Int. J. Pharm.*, 2011, **418**(1), 13–17.

46 J. Ding, Y. Hao, B. Liu, Y. Chen and L. Li, Development and application of poly(lactic acid)/poly(butylene adipate-*co*-terephthalate)/thermoplastic starch film containing salicylic acid for banana preservation, *Foods*, 2023, **12**(18), 3397.

47 O. P. Chauhan, P. S. Raju, D. K. Dasgupta and A. S. Bawa, Instrumental textural changes in banana (var. Pachbale) during ripening under active and passive modified atmosphere, *Int. J. Food Prop.*, 2006, **9**(2), 237–253.

48 P. H. Huang, Y. T. Cheng, W. C. Lu, P. Y. Chiang, J. L. Yeh, C. C. Wang, Y. S. Liang and P. H. Li, Changes in nutrient content and physicochemical properties of cavendish bananas var. pei chiao during ripening, *Horticulturae*, 2024, **10**(4), 384.

49 T. T. Alemu, Effect of storage time and room temperature on physicochemical and geometric properties of banana (Musa spp.) fruit, *J. Plant Biota*, 2023, 30–40.